Systematic study on propulsive performance of tandem hydrofoils for a wave glider

Fuming Yang, School of Naval Architecture and Ocean Engineering, Harbin Institute of Technology, Weihai, PR China

Weichao Shi, Department of Naval Architecture, Ocean and Marine Engineering, University of Strathclyde, U.K.

Dazheng Wang, School of Naval Architecture and Ocean Engineering, Harbin Institute of Technology, Weihai, PR China

*corresponding author: Fuming Yang

Address: School of Naval Architecture and Ocean Engineering, Harbin Institute of Technology, No.2, Wenhua West Road, Weihai, 264209, Shandong Province, China

E-mail address: 520118591@qq.com

Abstract: This paper presents the propulsive performance optimization of tandem hydrofoils equipped in a wave glider in head sea conditions with the aid of computational fluid dynamic (CFD) method by using a commercial CFD code, STAR-CCM+.

Firstly, this work performs a systematic study on a single 2D hydrofoil to study the effect of varying the pivot position and the torsional spring stiffness to seek for the optimum propulsive performance within a range of velocity. Secondly, parametric studies on the propulsive performance of 2D and 3D six tandem hydrofoils are conducted by varying the oscillation amplitude and the torsional spring stiffness.

The result reports: The results show that the torsional springs play a critical role in propulsive performance, comparing to the pivot position. The propulsive performance of the middle hydrofoil is greater than the others in the fore and after positions. When 2D and 3D six tandem hydrofoils achieve the optimum propulsive performance, the frequency ratio is chosen to be around 25 (torsional spring stiffness ($k_S = 0.8N \cdot m/rad$)) and 17 (torsional spring stiffness ($k_S = 11.8N \cdot m/rad$)), respectively. Comparing to previous study, the propulsive performance of each hydrofoil in six tandem hydrofoil configuration is greatly improved and none of hydrofoil produce negative thrust.

Keywords: wave glider, tandem hydrofoils, passive eccentric rotation, torsional spring

Nomenclature

H	is the wave height.
T	is the wave period.
k	is the wave number.
I_{hy}	is the inertia moment of hydrofoil.
$Q(t)$	is the resultant torque on the hydrofoil's pivot axis.
θ_{hy}	is the pitching angle of the hydrofoil
$X_{hy}(t)$	is the time-varying forces of the hydrofoil in the x direction.
F_{hy}	is the time-averaged value of $X_{hy}(t)$.
C_{hyT}	is the thrust coefficient of the hydrofoil.
C_{THCT}	is the thrust coefficient of tandem hydrofoils.
F	is the frequency ratio.
f	is the wave frequency.
f_n	is the hydrofoil natural frequency.
$f_{encounter}$	is the hydrofoil oscillation encounter wave frequency.
k_S	is the torsional spring stiffness.

1. Introduction

In 2011, a wave glider integrated with novel sensors successfully navigated through the Pacific Ocean and completed a marine environmental survey in a much wider spatial range and temporal scales which has proven its merits in long voyaging and low cost surveying (Villareal and Wilson (2014)). Since then, it has attracted researchers' attention from all over the world. As like other sea going vehicles, better propulsive performance of the wave glider is always desirable.

As the propulsor of the wave glider, the motion of tandem hydrofoils can be decomposed into the actuated plunging motion and the passive pitching motion. The propulsion of hydrofoil with passive pitching motion is affected by the pivot axis position, the inertia (density ratio of the hydrofoil and fluid), the hydrofoil section, the aspect ratio and the torsional spring stiffness (Isshiki (1982a, 1982b), Isshiki and Murakami (1983, 1984)). Pioneer Isshiki (1982a, 1982b) proposed a new concept of passive-type wave devouring propulsion using the hydrofoil. The experiments are conducted both in a short wave (wave length/hydrofoil chord=$3\sim8$) and a long wave range (wave length/hydrofoil chord=$5\sim20$) (Isshiki and Murakami (1983, 1984)). They find that the wave devouring efficiency of a hydrofoil without the consideration of the free surface effects increases monotonically as the depth of submergence decreases and the advanced speed increases. On the other hand, the pivot axis of the hydrofoil has a significant impact on the propulsion. The closer the pivot axis is to its leading edge, the greater the passive rotation angle of the hydrofoil is (Zhang and Lu (2009), Spagnolie et al. (2010)). When the hydrofoil rises, it does head-up rotation and vice versa. Zhang et al. (2010) employed a multi-block Lattice Boltzmann Method (LBM), a so-called lumped-torsional-flexibility dynamic model constructed by a rigid plate with a torsional spring acting on the pivot at the leading edge of the plate. They found a periodic status (including forward and backward) and a non-periodic status which is determined by linear density ratio and frequency ratio, defined as the hydrofoil natural frequency to the forced plunging frequency.

A systematic numerical investigation on a three-dimensional flapping rigid wing with passively actuated lateral and pitching motion about its pivot axis (from center to leading edge) was performed by Xiao et al. (2014). While the simulations are conducted under the conditions of aspect ratio (AR=1.0 to infinity), inertia (density ratio $\sigma = 4\sim32$), torsional stiffness (frequency ratio $F = 1.5\sim10$ and infinity) and pivot axis (from chord-center to leading edge). They found that the torsional stiffness definitely plays a role in the

overall hydrofoil dynamic response on two-degree-of-freedom lateral and pitching motion by comparison of one-degree-of-freedom lateral passive motion only. Moreover, the induced lateral velocity is fully dependent on the torsional stiffness. Furthermore, large AR wing generates greater forces and moments than a low AR one.

Two tandem hydrofoils effectively enhance the total force and reduce the drag compared to two independent wings (Zhang and Lu (2009)). Lua et al. (2016) conduct two 2D oscillating wings in tandem configuration in forward flight at a low Reynolds number to investigate the phase difference between the heave and pitching motion and the adjacent spacing impact on the aerodynamic performance and the corresponding flow structures. Both the fore wing and hind wing undergo same simple harmonic heaving and pitching motion with a Strouhal number of 0.32, phase angle ($-180^{o}\sim180^{\mathrm{o}}$) and four adjacent spacing ($\mathrm{s}=1.5\mathrm{c}\sim4c$, c is the wing chord length). They found that when $\mathrm{s}=2\mathrm{c}$, two tandem wings perform better than the sum of two independent wings. Moreover, the maximum thrust on the hind wing occurs during in-phase oscillating. As increasing the number of the hydrofoils, the overall propulsive performance can be better achieved. However, as the number of foils exceeds three, the growth rate of overall thrust generation declines (Yuan et al. (2015)). The study addressing the role of tandem flapping hydrofoils as a wave glider propulsor also has been pursued by Liu et al. (2016) numerically and experimentally. While simulations are carried out to investigate the hydrodynamic performance of 2D tandem asynchronous flapping foils (TAFFs) with varying the parameters of non-dimensional wave length and non-dimensional wave height but the pitching law of TAFFs is imposed and the plunging motions are activated. They found that the higher thrust force and input power at smaller wave length or larger wave height. Moreover, the flow interactions of adjacent hydrofoils are beneficial to improving the thrust force and efficiency.

Therefore, either tandem hydrofoils or the application of torsion spring acting on the pivot axis could enhance the overall propulsion performance. In order to obtain the optimum propulsion performance of the wave glider propulsor, the number of hydrofoils arranged in tandem and the stiffness of the torsion spring would be determined. The question of whether the hydrodynamic performance of imposing pitching motion applied by 2D tandem hydrofoils is identical to the hydrodynamic performance of passively induced pitching motion of 3D tandem hydrofoils, especially the application of the torsion spring, and this article provides new findings on this critical area.

In the present study, the purpose of this paper is to improve the propulsive performance of tandem hydrofoils for the wave glider. Within this framework, we firstly perform a comprehensive investigation on the hydrodynamic performance of 2D single hydrofoil with a forced plunging motion and passive pitching motion under different uniform lateral velocities to find out the optimum the torsion spring stiffness and the pivot position. Then, the hydrodynamic performance of 2D six tandem hydrofoils is studied to further optimize the torsion spring stiffness to obtain the best propulsive performance under same amplitude plunging motion. Finally, the method for obtaining the best propulsion performance of 2D six tandem hydrofoils is successful applied to 3D six tandem hydrofoils to achieve the best propulsive performance of tandem hydrofoils for the wave glider.

2. Brief description of the investigated wave glider

The wave glider model (Fig.1) used in this paper is the same as previous studies developed by China National Marine Technology Center (Yang et al. (2018)). Six tandem hinged flat hydrofoils are arranged in a straight line. The previous study has successful conducted numerical simulation and experimental validation of the wave glider in head seas. However, it was found that the propulsive performance of six tandem hydrofoils was not satisfactory; some of hydrofoils were even producing negative thrust. This paper is going to optimize the propulsive performance of six tandem hydrofoils under different forward velocities, with focus on improving the hydrofoil from providing negative thrust.

2.1 Motion characteristics

A three-dimensional rectangular hydrofoil model is depicted in Fig.2. As defined in the figure, c and b is the chord and span of hydrofoil, respectively. The hydrofoil is immersed in a uniform upstream velocity U_∞ and time-varying velocity vector $V(t)$, while the pitching (θ) motion is solved by the fluid-structure interaction solver to couple the force acted by the surrounded fluid as well as the spring and the hydrofoil motion. A specified sinusoidal velocity $V(t)$ in the vertical direction which is defined as

$$V(t) = 2\pi a f_{encounter} \sin(2\pi f_{encounter} t) \tag{1}$$

$$f_{encounter} = f + kU_\infty cos\alpha \tag{2}$$

Where a is the oscillation amplitude of the hydrofoil , $f_{encounter}$ is the wave glider encounter wave frequency, f is the wave frequency, k is wave number, U_∞ is the lateral velocity and α is the heading angle (head wave is 180°). Each hydrofoil in the tandem hydrofoils has a rectangular cross-section and the thickness of the hydrofoil is $0.02\mathrm{m}$. Tandem hydrofoils are arranged in-line and the distance between the tailing edge of a foil and the leading edge of the downstream one is 0.02m.

Passive pitching motion of the hydrofoil is governed by a rotational momentum equation as based on a torsion spring acting about the pivot axis:

$$I_{hy} d^2\theta(t)/dt^2 + k_S \theta_{hy} = Q(t) \tag{3}$$

Where I_{hy} is the inertia moment of hydrofoil, θ_{hy} is the pitching angle of the hydrofoil and

k_S is the torsional spring stiffness; $Q(t)$ is the resultant torque on the pivot axis.

2.2 Parameter definition

The average thrust (F_{hy}) of the hydrofoil has been defined as:

$$F_{hy} = \int_0^T X_{hy}(t)\, dt/T \tag{4}$$

Where $X_{hy}(t)$ is the hydrofoil time-varying forces in the horizontal direction.

The average thrust coefficient (C_{hyT}) of the hydrofoil have been defined as:

$$C_{hyT} = F_{hy}/0.5\rho U_\infty^2 S_{hy} \tag{5}$$

Where S_{hy} represents the area of the hydrofoil, $S_{hy} = bc$.

In the numerical simulation of six tandem hydrofoils, the average thrust coefficient of six tandem hydrofoils configuration (C_{THCT}) have been also defined as:

$$C_{THCT} = \sum C_{hyT}\,/6 \tag{6}$$

Where $\sum C_{hyT}$ represents the total thrust coefficient of six tandem hydrofoils.

To evaluate torsion spring effect on the propulsive performance of six tandem hydrofoils with torsion spring, non-dimensional parameter frequency ratio (F) is introduced to represent the torsional stiffness is defined as

$$F = f_n/f_{encounter} \tag{7}$$

Where f_n is the hydrofoil natural frequency defined as

$$f_n = \sqrt{k_S/I_{hy}}\,/2\pi \tag{8}$$

The average input power (P_i) of the hydrofoil is defined as:

$$P_i = (\int_0^T Z_{hy}(t)\, V(t) dt)/T_n \tag{9}$$

Where $Z_{hy}(t)$ is the hydrofoil time-varying forces in the vertical direction.

The average input power coefficient (C_{pi}) of the hydrofoil is also defined as:

$$C_{pi} = P_i/0.5\rho U_{\infty}^3 S_{hy} \tag{10}$$

Similarly, the average input power coefficient of six tandem hydrofoils configuration (C_{THPI}) have been also defined as:

$$C_{THPI} = \sum C_{pi}/6 \tag{11}$$

Where $\sum C_{pi}$ represents the total input power coefficient of six tandem hydrofoils.

The oscillation amplitude of the tandem hydrofoils can characterize the ability of the surface boat to absorb wave energy, the maximum average input power (P_m) of the hydrofoil under different oscillation amplitudes have been defined as:

$$P_m = \rho g(2a)^2 S_f/8\mathrm{T}_n = \rho g a^2 S_f/2\mathrm{T}_n \tag{12}$$

Where S_f represents the waterplane area of the surface boat.

The maximum average input power coefficient (C_{pm}) of the hydrofoil is also defined as:

$$C_{pm} = P_m/3\rho U_{\infty}^3 S_{hy} \tag{13}$$

3. Numerical simulation methodology of tandem hydrofoils

3.1 Boundary conditions

The simulation of 2D and 3D hydrofoil is conducted with the boundary conditions defined in Fig.3 (a) and Fig.3 (b). Uniform static pressure is applied to the outlet condition at 1m (2D) and 3.5m (3D) downstream. Since the hydrofoil has a chord length of 0.16m, the distance between the outlet and nearest hydrofoil is larger than five times the hydrofoil chord length. Thus, non-physical reflection from the outlet is avoided. The time-varying velocity vector is applied to top and bottom condition and uniform incoming velocity is applied to inlet condition. The thickness between the symmetry plane 1 and symmetry plane 2 of 2D

hydrofoil is 0.02m. This ensures that the passive pitching motion of the hydrofoil is simulated by applying overset grid techniques. No-slip boundary conditions are applied to the tandem hydrofoils. Each hydrofoil is immersed in the rectangular center domain and the interface is created between adjacent hydrofoil domains.

3.2 Mesh generation

As shown in Fig.4 (a) and Fig.4 (b), overset mesh is applied to rectangular domain of the hydrofoil is also applied to simulate the passive eccentric rotation. The target height of the first cell near the wall is to keep the wall $y^+ < 1$. The total mesh number and vertices of the single and tandem hydrofoils in 2D and 3D as listed in Table 1.

3.3 Validation and sensitivity study

Prior to conducting a detailed simulation, the grid independence tests of 2D and 3D oscillating tandem hydrofoils cases has been done in our previous work (Yang et al. (2018)). Comparisons with existing experimental and computational results cover the predictions of time-mean thrust coefficients and time-independent thrust coefficients. The comparison of the results indicates that there is a good agreement between the results of oscillating hydrofoils and the published results of Kinsey and Dumas (2012).

4. Parametric study on propulsion performance of tandem hydrofoils

In previous study (Yang et al. (2018)), we identified the propulsive performance of each hydrofoil in the six tandem hydrofoils based on sea state 2 (H=0.17m, T=2s). However, the thrust of the second hydrofoil was found to be negative. According to equations (1) to (3), the propulsion performance of the tandem hydrofoils is affected by both physical design factors (pivot position and hydrofoil stiffness) and external environmental factors (amplitude and encounter frequency), where the lateral velocity directly determines the encounter frequency.

In order to study the influence of physical design factors on the propulsion performance of the tandem hydrofoils and avoid the effects of hydrodynamic forces between adjacent hydrofoils, in this section, a detailed parametric study on 2D single hydrofoil has been conducted to decide the pivot position and the frequency ratio (variation of the hydrofoil stiffness) to optimize the induced pitching angle and the thrust

force coefficient under three different uniform lateral velocities in Section 4.1. In terms of external environmental factors, section 4.2 extends to investigate to 2D six tandem hydrofoils propulsion performance by varying the frequency ratio (*F*). The optimized torsional spring stiffness on the propulsion performance of 3D six tandem hydrofoils and the parameter for obtaining the best propulsive performance of 3D six tandem hydrofoils are further discussed in section 4.3.

4.1 2D single hydrofoil

The hydrofoil is immersed in a field with the lateral velocity U_∞ and the time-varying vertical vector $V(t)$, while the pitching (θ) motion is passively forced by the wave action. To better evaluate the propulsion performance of the hydrofoil, three lateral velocities ($U_\infty = 0.20\ m/s, 0.35\ m/s, 0.60\ m/s$) are chosen for the numerical simulations of the hydrofoil. Numerical simulations of the hydrofoil are conducted with various pivot positions ($x/c = 0, 0.25, 0.3125$; x is distance between the pivot axis and leading edge of the hydrofoil) and frequency ratios ($F = 0{\sim}10.62$). The density ratio of the hydrofoil and fluid is set to 1. The oscillation amplitude is $H/2$.

4.1.1 Pivot position effect

The position of pivot does not only determine the pitching motion of the hydrofoil but also affect the thrust coefficient. The average thrust coefficient under different pivot positions for 2D single hydrofoil are shown in Fig.5. It is clear that the hydrofoil with the pivot axis at the leading edge ($x/c = 0$) do not produce much forward thrust under the three velocities. However, when the pivot axis moves away from the leading edge ($x/c = 0.25, 0.3125$), the hydrofoil produces forward thrust when the lateral velocity is 0.2 m/s and 0.35 m/s, especially when $x/c = 0.3125$; as the lateral velocity increases, the thrust declines sharply and produces even backward forces.

Furthermore, the pivot axis also affects the passive pitching angle as shown in Fig.6. It is important to highlight the fact that the hydrofoil with the pivot axis at the leading edge has larger pitching angle at the initial moment ($t/T = 0$). However, when the pivot position is 0.3125, the pitching angle is around 0^o at the initial moment, and then it returns to initial state after periodic rotation. It implies that the variation of the pivot bias distance could determine the phase difference between the heave motion and the pitching motion.

As the lateral velocity increases, the induced pitch motion of the hydrofoil with the pivot position $x/c = 0.3125$ becomes unsteady, especially $U_\infty = 0.6\ m/s$. The thrust coefficient plunges drastically.

Therefore, the hydrofoil with the pivot axis away from the leading edge achieves a better propulsion performance, this is why the pivot bias distance in previous study was chosen to be 0.3125, and the need for optimization in this paper due to the large negative thrust generated as the lateral velocity increases.

4.1.2 Torsion spring effect

The torsion spring acting on the pivot axis could constrain the pitching motion and also manipulate the passive pitching motion. The results summarized in Fig.7 presents all the average thrust coefficients of 2D single hydrofoils with different pivot positions and different torsional spring stiffness (which results in a range of various frequency ratios, F) operating under a range of lateral velocities.

The hydrofoil with torsion spring achieves better propulsive performance than the hydrofoil without torsion spring, especially for the hydrofoil with the pivot position $x/c = 0$ for which torsion spring essentially overturns the thrust from negative to positive. However, the average thrust coefficient of the hydrofoil with the pivot axis located in $x/c = 0.25, 0.3125$ is still negative when the lateral velocity is 0.6 m/s; it implies that the torsion spring does not fundamentally improve the propulsion performance of the hydrofoil with the pivot position ($x/c = 0.25, 0.3125$). But, the average thrust coefficient of the hydrofoil with the pivot position $x/c = 0$ increases first and decreases under three lateral velocities, and the maximum average thrust coefficient is larger than the other pivot positions ($x/c = 0.25, 0.3125$) at the same lateral velocity. It indicates that the hydrofoil with the torsion spring and the pivot position $x/c = 0$ has better propulsive performance.

The hydrofoil with torsion spring acting on the pivot axis also influences the passive pitching motion. The passive pitching motion of 2D single hydrofoil with the pivot axis at the leading edge under various frequency ratios (*F*) is shown in Fig.8. From the results, it is clear that the maximum pitching angle gradually decreases as the lateral velocity increases. The passive pitching motion of the hydrofoil under higher frequency ratios ($F = 4.82, 5.39, 5.90$) is getting converged with similar amplitude.

Fig.9 show evolution of instantaneous thrust coefficient and velocity contour of 2D single hydrofoil with oscillation amplitude of $H/2$. Periodic thrust is generated. Flow separation occurs at the trailing edge of the

hydrofoil especially in the lower speed due to the large angle of attack; as the lateral velocity increases, the separation gradually improves.

Based on the above simulation, the pivot position $x/c = 0$ the configuration where the torsion spring acts on the pivot axis and the pivot axis is at the leading edge is used in the following numerical simulation.

4.2 Torsional spring stiffness optimization for 2D six tandem hydrofoils

4.2.1 Oscillation amplitude effect

The oscillation amplitude of the hydrofoil expresses the ability of the boat to absorb wave energy. The vertical oscillating amplitudes of the 2D six tandem hydrofoils is $H/2$, $3H/8$ and $H/4$. The higher oscillation amplitude ($H/2$) is that the surface boat moves with wave, however, the surface boat cannot fully move with wave when the characteristic length of the surface boat is less than one-seventh of the wave length (Salvesen (1970)), thus different oscillation amplitudes are selected for studying the propulsion performance of tandem hydrofoils. The hydrofoil in the six tandem hydrofoils configuration is numbered HY-1, HY-2, HY-3, HY-4, HY-5 and HY-6 from stem to stern. The torsion spring is mounted on the leading edge of the hydrofoil ($x/c = 0$). The frequency ratio is from 5 to 30. The lateral velocities is set to $0.20m/s$.

Fig.10 shows the average thrust coefficient of 2D six tandem hydrofoils with different oscillation amplitudes. As the frequency ratio increases, the average thrust coefficient of tandem hydrofoil increases and then decreases. Further increasing the frequency ratio (*F*) doesn't have significant improvement in thrust. Moreover, when tandem hydrofoils achieve the best propulsive performance under the lateral velocity of 0.2 m/s and three different oscillation amplitudes, the frequency ratio (*F*) is 25.63 ($k_s = 0.8N \cdot m/rad$), 25.63 ($k_s = 0.8N \cdot m/rad$) and 22.20 ($k_s = 0.6N \cdot m/rad$), respectively. Therefore, the frequency ratio is from 22 to 26, which helps the 2D tandem hydrofoils to achieve excellent propulsive performance. Furthermore, when the oscillation amplitude is reduced by 12.5%, the average thrust coefficient of the hydrofoil is reduced by 32.2% (from $H/2$ to $3H/8$) and 55.5% (from $3H/8$ to $H/4$), respectively, as shown in Table 2. This means that as the amplitude of the oscillation decreases, the propulsion performance of the hydrofoil deteriorates significantly.

Fig.11 summarizes the maximum average thrust coefficient of each hydrofoil with different oscillation amplitudes selected from Fig.10. As the oscillation amplitude increases, the propulsive performance of each hydrofoil in the tandem hydrofoils is enhanced, especially the hydrofoil arranged in the middle. Another

promising finding is that all hydrofoil is provide positive thrust.

Similar to the single hydrofoil, Fig.12 shows the passive pitching angle of tandem hydrofoils. The passive pitching angle of the hydrofoil directly impacts the propulsive performance of the hydrofoil. If the average thrust coefficient of the tandem hydrofoils is maximized, the maximum passive pitching angle with different oscillation amplitudes are in the range of $5^{o}\sim15^{o}$. Furthermore, the passive pitching angle of the hydrofoil arranged in the middle of tandem hydrofoils is greater than that of the stem and stern hydrofoil and shows more stable sinusoidal movement.

4.2.2 Lateral velocity effect

According to equation (3), the frequency of the oscillation frequency increases as the lateral velocity increases, which will eventually lead to the difference in propulsion performance of the 2D tandem hydrofoil. As shown in Fig.13, the maximum average thrust coefficient of 2D tandem hydrofoils appears in the frequency ratio of 25 to 30, as shown in Table 3. According to equation (5), the average thrust coefficient of 2D tandem hydrofoil is inversely proportional to the lateral velocity; therefore, the average thrust coefficient of 2D tandem hydrofoils increases by 10.05% (0.20 m/s to 0.35 m/s) and -27.44% (0.35 m/s to 0.60 m/s), respectively. This indicates that as the lateral velocity increases, the average thrust coefficient of 2D tandem hydrofoils increases first and then decreases, and it also implies that the increase of the oscillation frequency does not continuously improve the propulsion performance of the hydrofoil.

Similarly, as the lateral velocity increases, the propulsive performance of the hydrofoil arranged in the middle is better than that of stern hydrofoil and the maximum passive pitching angle are in the range of $5^{o}\sim15^{o}$, as shown in Fig.14 and Fig.15.

From the discussion of the propulsive performance of 2D six tandem hydrofoils, the propulsive performance of 2D six tandem hydrofoils is significantly enhanced compared to six independent single hydrofoils. If the tandem hydrofoils achieves the optimum propulsive performance under different oscillation amplitudes and lateral velocities, the frequency ratio of 2D six tandem hydrofoils is chosen to be around 25 ($k_s = 0.8N \cdot m/rad$); considering three-dimensional effect at the hydrofoil tip, the maximum frequency ratio of the following numerical simulation of 3D tandem hydrofoils is less than 25.

4.2.3 Detailed flow analysis for 2D tandem hydrofoils in the passive pitching motion

From Fig.16 show the evolution of instantaneous thrust coefficient and velocity contour of 2D six tandem hydrofoils with oscillation amplitude of $H/2$, $3H/8$ and $H/4$ when 2D six tandem hydrofoils have the

best propulsive performance, respectively. When at the instant of 0 ($t/T = 0$), 2D six tandem hydrofoils is at the crest and is about to move downwards; while at the instant of 0.5 ($t/T = 0.5$), 2D tandem hydrofoils is at the trough and moves toward the crest. Higher velocity appears between adjacent hydrofoils, especially the hydrofoil arranged in the middle of the tandem hydrofoils at the instant of t/T =0.25 and 0.75. That is the reason why the propulsion performance of the middle of the hydrofoil in tandem hydrofoils is larger than those of the hydrofoil in stem and stern because of the slat effect. Furthermore, similar to 2D single hydrofoil, the optimum thrust coefficient of 2D six tandem hydrofoils appears at the instant of 0.25 and 0.75.

4.3 Torsional spring stiffness optimization for 3D six tandem hydrofoils

4.3.1 Difference between the hydrodynamic performance of 2D and 3D six tandem hydrofoils

Fig. 17 shows the average thrust coefficient of 2D and 3D six tandem hydrofoils with different oscillation amplitudes operating under three lateral velocities, respectively. There is significantly difference between the average thrust coefficient of 2D and 3D six tandem hydrofoils. Furthermore, if the propulsive performance of six tandem hydrofoils achieve the best, the frequency ratio required for the 3D six tandem hydrofoils is smaller than that of the 2D six tandem hydrofoils. Comparing to 2D six tandem hydrofoils, when the lateral velocity is 0.2 m/s and three different oscillation amplitudes, the frequency ratio is 18.09 ($k_s = 11.8N \cdot m/rad$), 18.09 ($k_s = 11.8N \cdot m/rad$) and 12.79 ($k_s = 5.9N \cdot m/rad$),respectively. Similarly, when the lateral velocity is 0.35m/s and three different oscillation amplitudes, the frequency ratio is 21.23 ($k_s = 17.75N \cdot m/rad$),17.31 ($k_s = 11.8N \cdot m/rad$) and 12.24 ($k_s = 5.9N \cdot m/rad$), respectively; when the lateral velocity is 0.35m/s and three different oscillation amplitudes, the frequency ratio is 16.15 ($k_s = 11.8N \cdot m/rad$). Therefore, the frequency ratio is from 12 to 22, which helps the 3D tandem hydrofoils to achieve excellent propulsive performance.

Fig.18 summarizes the average thrust coefficient of each hydrofoil in the maximum average thrust coefficient of six tandem hydrofoils with different oscillation amplitudes selected from Fig.17. It is clearly that the average thrust of the hydrofoil in the middle of six tandem hydrofoils (from HY-2 to HY-5) is larger than that of the hydrofoil in stem and stern (HY-1 and HY-6). The passive induced pitching angle of the HY-1 and HY-6 is smaller than those of the hydrofoil from HY-2 to HY-5 in Fig.20.

Therefore, both the 2D and 3D six tandem hydrofoils also perform outstanding propulsive performance. However, if the 3D six tandem hydrofoils achieves excellent propulsion performance, the frequency ratio is

about 17 ($k_s = 0.8N \cdot m/rad$); compared to 2D tandem hydrofoil, 3D tandem hydrofoils needs to reduce the frequency ratio (torsional spring stiffness) to obtain the optimum propulsive performance and the frequency ratio needs to be reduced to 68% of 2D tandem hydrofoils.

4.3.2 Detailed flow analysis for 3D tandem hydrofoils in the passive pitching motion

From Fig.19 to Fig.24 show the evolution of instantaneous thrust coefficient and velocity contour of 3D six tandem hydrofoils with oscillation amplitude of $H/2$, $3H/8$ and $H/4$ when 3D six tandem hydrofoils have the best propulsion performance, respectively. When at the instant of 0 ($t/T = 0$), 3D six tandem hydrofoils is at the crest and is about to move downwards; while at the instant of 0.5 ($t/T = 0.5$), 3D six tandem hydrofoils is at the trough and moves toward the crest. Each row of velocity contour represents the same cross section of 3D six tandem hydrofoils; $y/b = 0.1871$ is close to the root of the hydrofoil, $y/b = 0.3371$ is at the center of the hydrofoil and $y/b = 0.4871$ is close to the hydrofoil tip. Comparing with the 2D six tandem hydrofoils, the thrust coefficient of 3D six tandem hydrofoils is greatly reduced due to the three-dimensional effect at the hydrofoil tip and the maximum drop is approximately 50%. This also can be clearly found from Fig.25. In addition, it can be intuitively found that the passive induced pitching angle of 3D six tandem hydrofoils under the oscillation amplitude of $H/4$ is smaller than those of the hydrofoil oscillation amplitude of $H/2$, and the thrust coefficient is reduced. Furthermore, as the cross section of the hydrofoil approaches its tip, the larger velocity region around tandem hydrofoils gradually shrinks, which explains why the 3D six tandem hydrofoils has lower propulsive performance compared to the 2D six tandem hydrofoils.

4.3.3 The choice of torsional spring stiffness

In order to achieve the best propulsion performance of the 3D tandem hydrofoils, there should be sufficient supplement for this purpose. According to equation (12), both the reduction in the oscillation amplitude and the increase in lateral velocity would reduce the input power required by the tandem hydrofoils. It is shown in Fig.26 that the average input power coefficient increases significantly with the increase of the torsional spring stiffness. This means that the tandem hydrofoils needs to consume more energy to get the best propulsion performance (the diamond mark on the solid curve). For the surface boat with unit waterplane area (previous study), if the surface boat moves vertically with the wave, the maximum average input power coefficient of the 3D tandem hydrofoils (green dotted line) is much less than the required

average input power coefficient (the red diamond mark on the solid curve); when reducing the frequency ratio ($F < 6.5$), the required average input power coefficient is less than the maximum value. Furthermore, it can be found that as the waterplane area of the surface boat increases, the maximum average input power coefficient increases; when the waterplane area increases to 4 m^2 (red, green and blue dotted line), the 3D tandem hydrofoils achieves the best propulsion performance regardless of the three different lateral velocities or oscillation amplitudes, which also implies that the surface boat fully moves with the wave. Therefore, when the input power is insufficient, the optimal propulsion performance of 3D tandem hydrofoils can be obtained by reducing the torsional spring stiffness or increasing the waterplane area of the surface boat.

5. Conclusions

In present study, the propulsion performance of the wave glider propulsor is optimized by changing the pivot axis location, torsion spring with the aid of STAR-CCM+. Firstly, a systematic study is performed on a single 2D hydrofoil to study the effect of varying the pivot position and the torsional spring stiffness to seek for the optimum propulsive performance. Secondly, parametric studies on the propulsive performance of 2D six tandem hydrofoils are conducted by varying the oscillation amplitude and the torsional spring stiffness. Finally, the simulation of 3D six tandem hydrofoil has been conducted with the optimum torsional spring stiffness to seek for the optimum propulsive performance. Therefore, conclusions haven been drawn as follows:

1. The best propulsion performance of 2D single hydrofoil is achieved by setting the pivot axis on the leading edge and applying the torsion spring on the pivot axis.

2. Comparing to six independent single hydrofoils, the propulsive performance of 2D tandem hydrofoil is further enhanced and the frequency ratio is chosen to be around 25 ($k_S = 0.8N \cdot m/rad$) when 2D six tandem hydrofoils achieves the optimum propulsive performance.

3. If the 2D and 3D tandem hydrofoils achieve the best propulsion performance, the oscillation amplitude of should be close to half of the wave height. Furthermore, when the lateral velocity is around 0.35 m/s, the maximum average thrust coefficient of the 2D and 3D tandem hydrofoil is obtained.

4. The propulsion performance of 3D tandem hydrofoils is greatly reduced due to the three-dimensional

effect at the hydrofoil tip and the maximum drop is approximately 50%. The frequency ratio is chosen to be around 17 ($k_s = 11.8N \cdot m/rad$) when 3D six tandem hydrofoils achieves the optimum propulsive performance. Furthermore, as the cross section of the hydrofoil closes to its tip, 3D six tandem hydrofoils has lower propulsive performance because of the larger velocity region around tandem hydrofoils gradually shrinks.

5. The propulsive performance of each hydrofoil in six tandem hydrofoils is improved and the hydrofoil does not provide negative thrust. The propulsion performance of the middle of the hydrofoil in tandem hydrofoils is better than those of the hydrofoil in stem and stern because of the slat effect.

6. The propulsion performance of the 3D tandem hydrofoils is also constrained by the maximum input power; when the input power of the 3D tandem hydrofoils is insufficient, reducing the torsion spring stiffness and increasing the waterplane area of the surface boat can effectively improve the propulsion performance of the 3D tandem hydrofoils.

Acknowledgment

Thanks are due to the National Ocean Technology Center [grant numbers:2014AA09A507] for funding the research.

Reference

Isshiki, H., 1982a. A Theory of Wave Devouring Propulsion (1St Report). Journal of the Society of Naval Architects of Japan. 1982(151), 54 - 64.

Isshiki, H., 1982b. A Theory of Wave Devouring Propulsion (2Nd Report). Journal of the Society of Naval Architects of Japan. 1982(152), 89 - 100.

Isshiki, H., Murakami, M., 1983. A Theory of Wave Devouring Propulsion (3Rd Report). Journal of the Society of Naval Architects of Japan. 1983(154), 118 - 128.

Isshiki, H., Murakami, M., 1984. A Theory of Wave Devouring Propulsion (4Th Report). Journal of the Society of Naval Architects of Japan. 1984(156), 102 - 114.

Kinsey, T., Dumas, G., 2012. Computational Fluid Dynamics Analysis of a Hydrokinetic Turbine Based On Oscillating Hydrofoils. Journal of Fluids Engineering, Transactions of the ASME. 134(2)

Liu, P., Su, Y., Liao, Y., 2016. Numerical and Experimental Studies On the Propulsion Performance of a Wave Glide Propulsor. China Ocean Eng. 30(3), 393-406.

Lua, K.B., Lu, H., Zhang, X.H., Lim, T.T., Yeo, K.S., 2016. Aerodynamics of Two-Dimensional Flapping Wings in Tandem Configuration. Phys Fluids. 28(12)

Salvesen, N., 1970. Ship Motions and Sea Load. Transactions of Sname. 78

Spagnolie, S.E., Moret, L., Shelley, M.J., Zhang, J., 2010. Surprising Behaviors in Flapping Locomotion with Passive Pitching. Phys Fluids. 22(4), 1-20.

Villareal, T.A., Wilson, C., 2014. A Comparison of the Pac-X Trans-Pacific Wave Glider Data and Satellite Data (Modis, Aquarius, Trmm and Viirs). Plos One. 9(3), e92280.

Xiao, Q., Hu, J., Liu, H., 2014. Effect of Torsional Stiffness and Inertia On the Dynamics of Low Aspect Ratio Flapping Wings. Bioinspir. Biomim. 9(0160081)

Yang, F., Shi, W., Zhou, X., Guo, B., Wang, D., 2018. Numerical Investigation of a Wave Glider in Head Seas. Ocean Eng.

Yuan, C., Liu, G., Ren, Y., Dong, H., 2015. Propulsive Performance and Vortex Interactions of Multiple Tandem Foils Pitching in Line., Dallas, TX, United states.

Zhang, J., Liu, N., Lu, X., 2010. Locomotion of a Passively Flapping Flat Plate. J. Fluid Mech. 659, 43-68.

Zhang, J., Lu, X., 2009. Aerodynamic Performance Due to Forewing and Hindwing Interaction in Gliding Dragonfly Flight. Physical Review E - Statistical, Nonlinear, and Soft Matter Physics. 80(1)

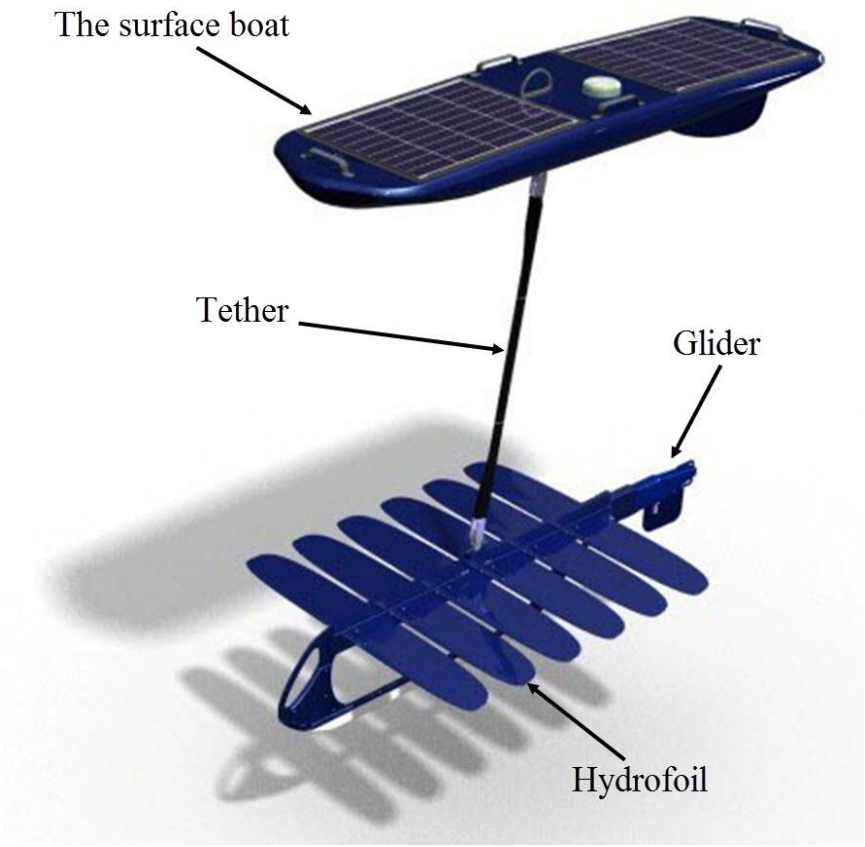

Fig.1. The wave glider developed by China National Marine Technology Center

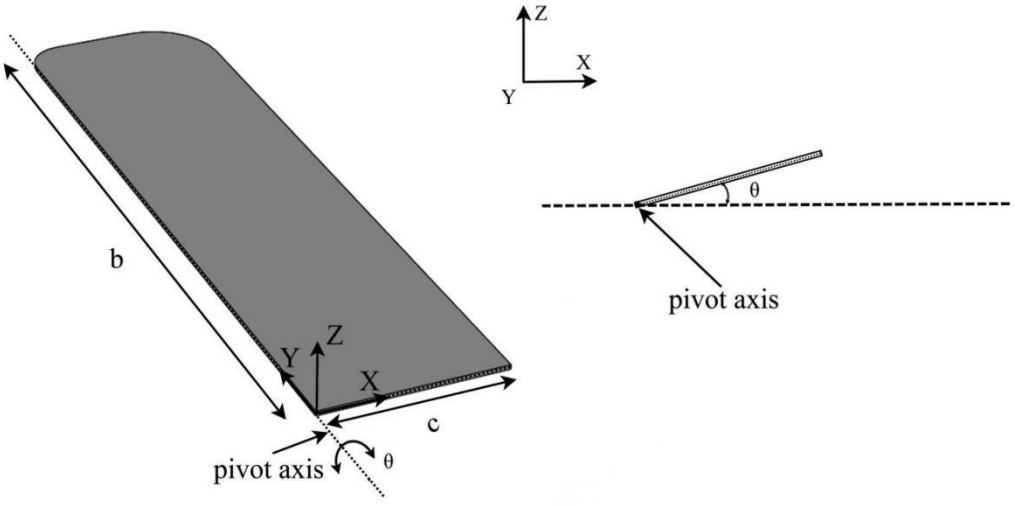

Fig.2. Sketch of a three-dimensional hydrofoil

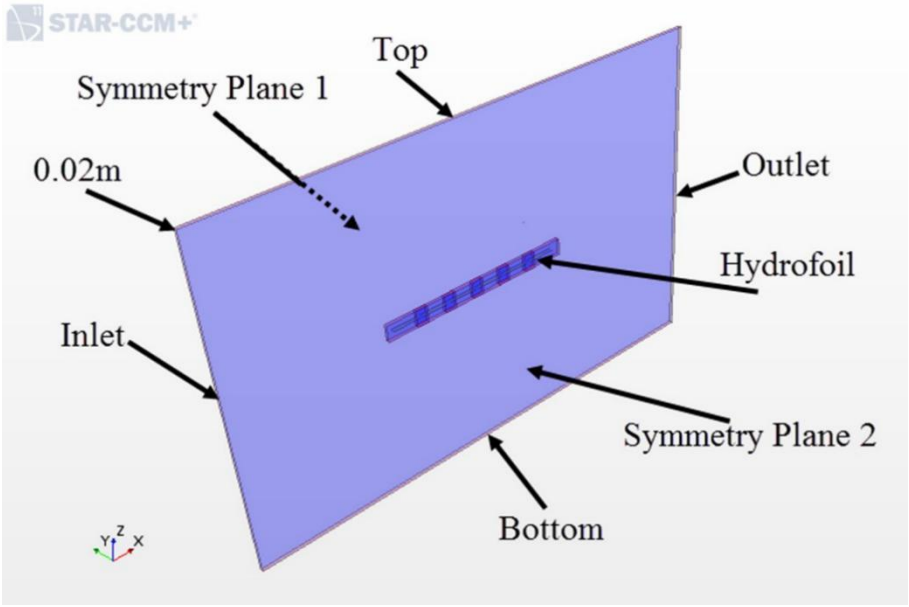

Fig.3 (a). Domain size and boundary condition for the passive eccentric rotation of 2D six hydrofoils

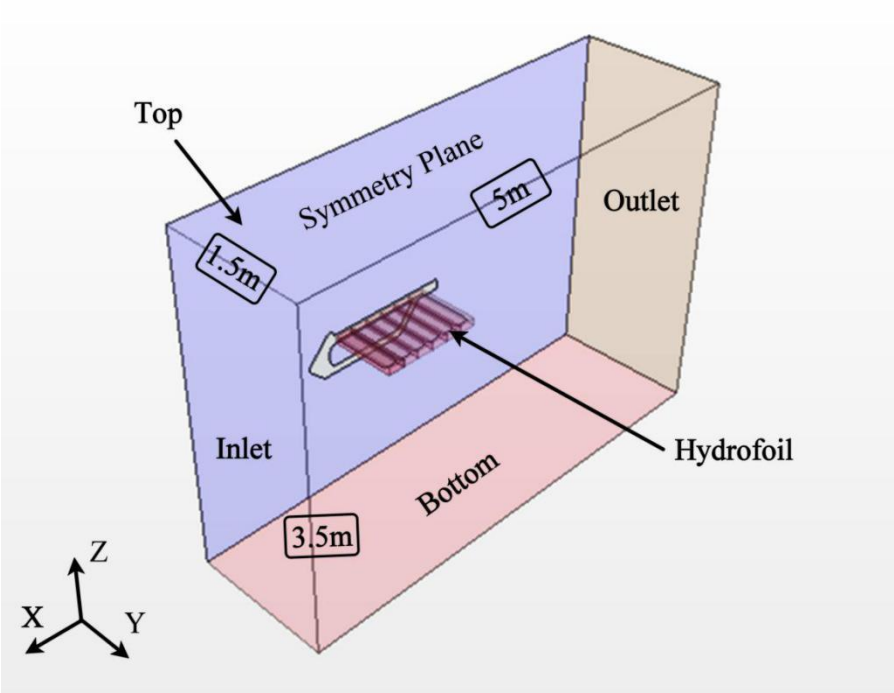

Fig.3 (b). Domain size and boundary condition for the passive eccentric rotation of 3D six tandem hydrofoils

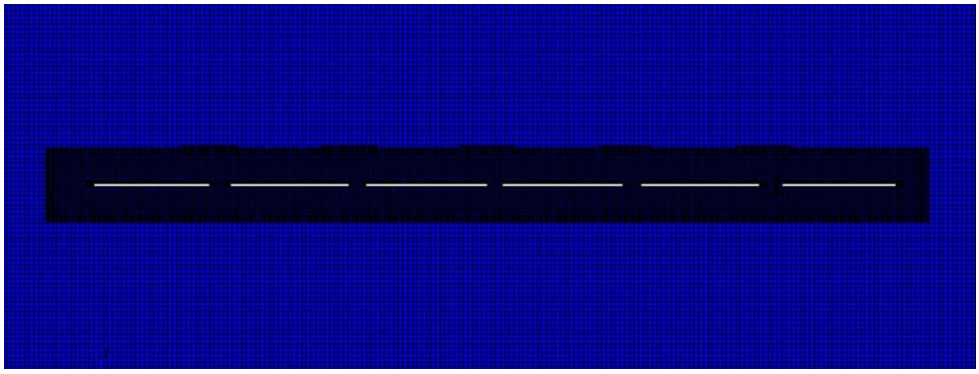

Fig.4 (a). The close-up view of 2D six tandem hydrofoils grid

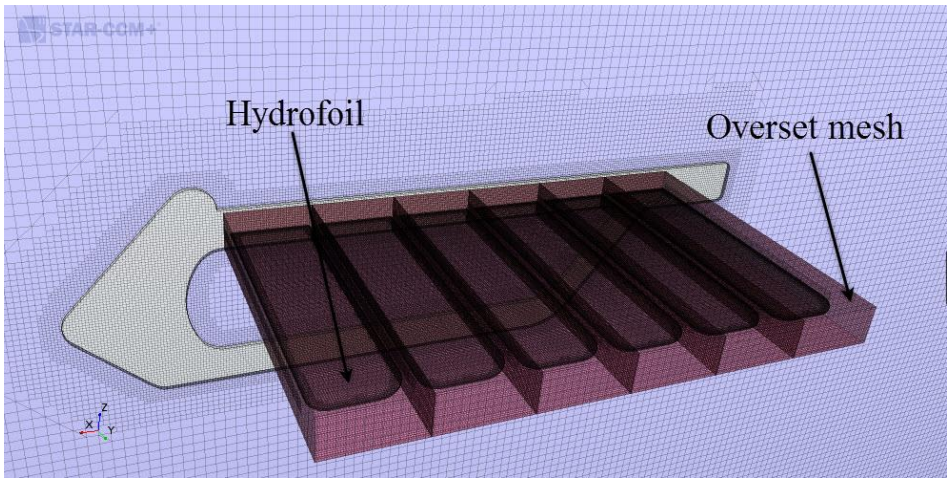

Fig.4 (b). The close-up view of 3D six tandem hydrofoils grid

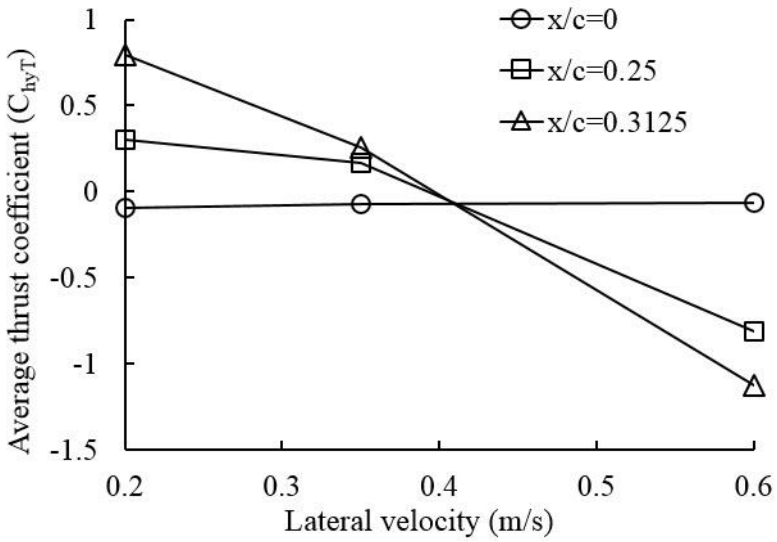

Fig.5. The average thrust coefficient of 2D single hydrofoil without torsional spring under different pitching bias distances

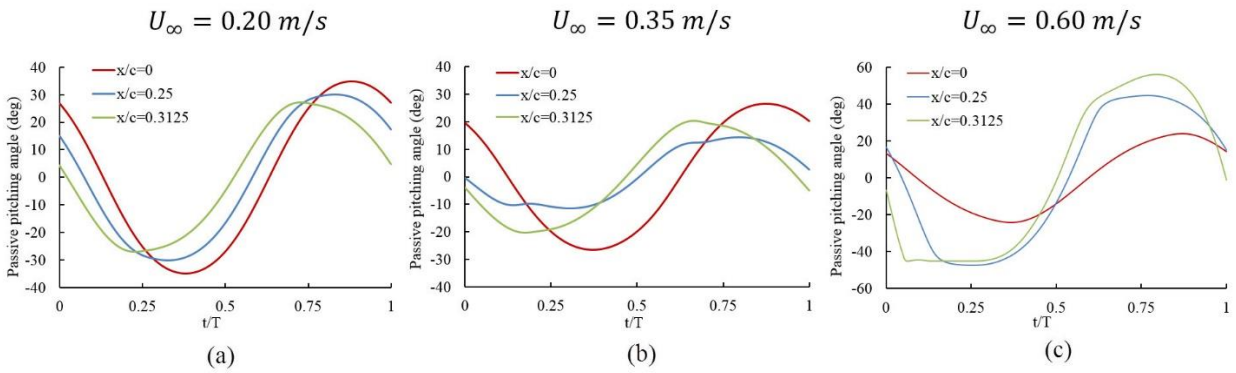

Fig.6. Variation of induced instantaneous pitching angle of 2D single hydrofoil without torsional spring.

(a) U_∞=0.2 m/s (b) U_∞=0.35 m/s (c) U_∞=0.6 m/s

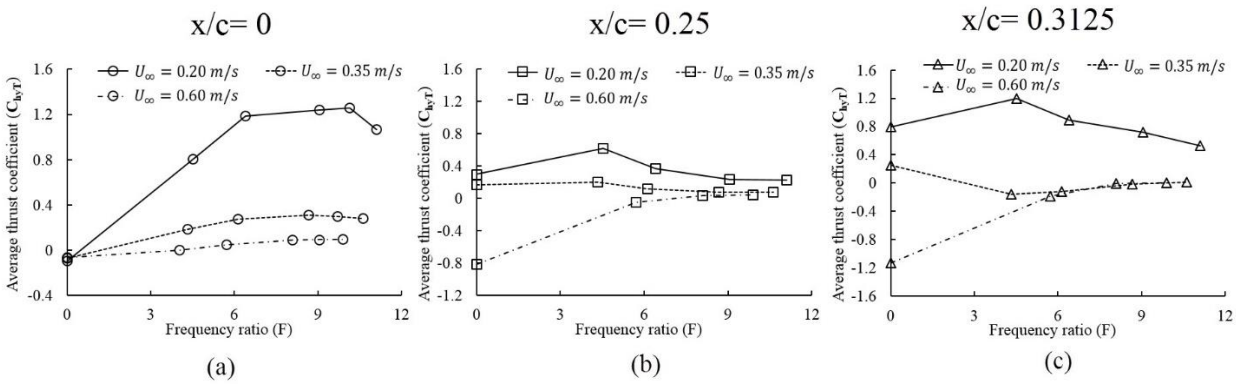

Fig.7. Variation of the average thrust coefficient of 2D single hydrofoil with torsional spring. (a) $x/c = 0$

(b) $x/c = 0.25$ (c) $x/c = 0.3125$

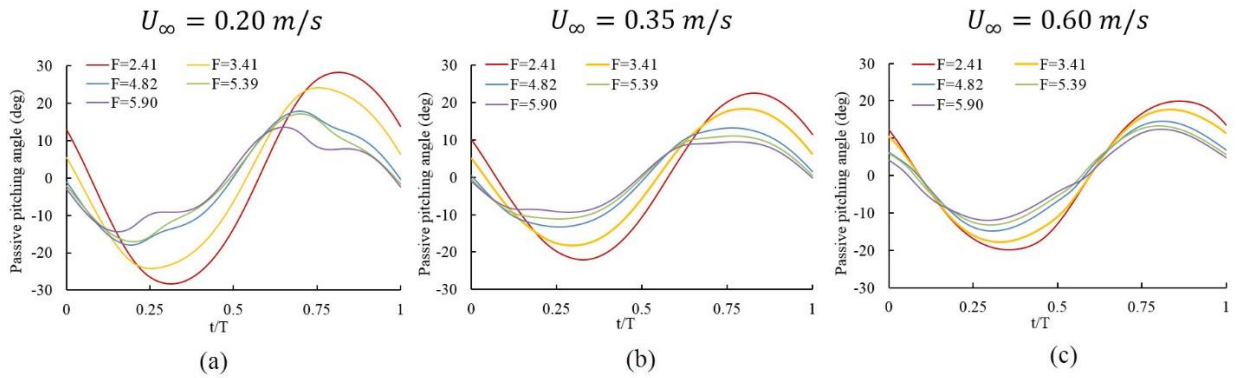

Fig.8. Variation of induced instantaneous pitching angle of 2D single hydrofoil with oscillation amplitude of H/2 and the pivot axis at the leading edge when 2D single hydrofoil has the best propulsion performance.

(a) U_∞=0.2 m/s (b) U_∞=0.35 m/s (c) U_∞=0.6 m/s.

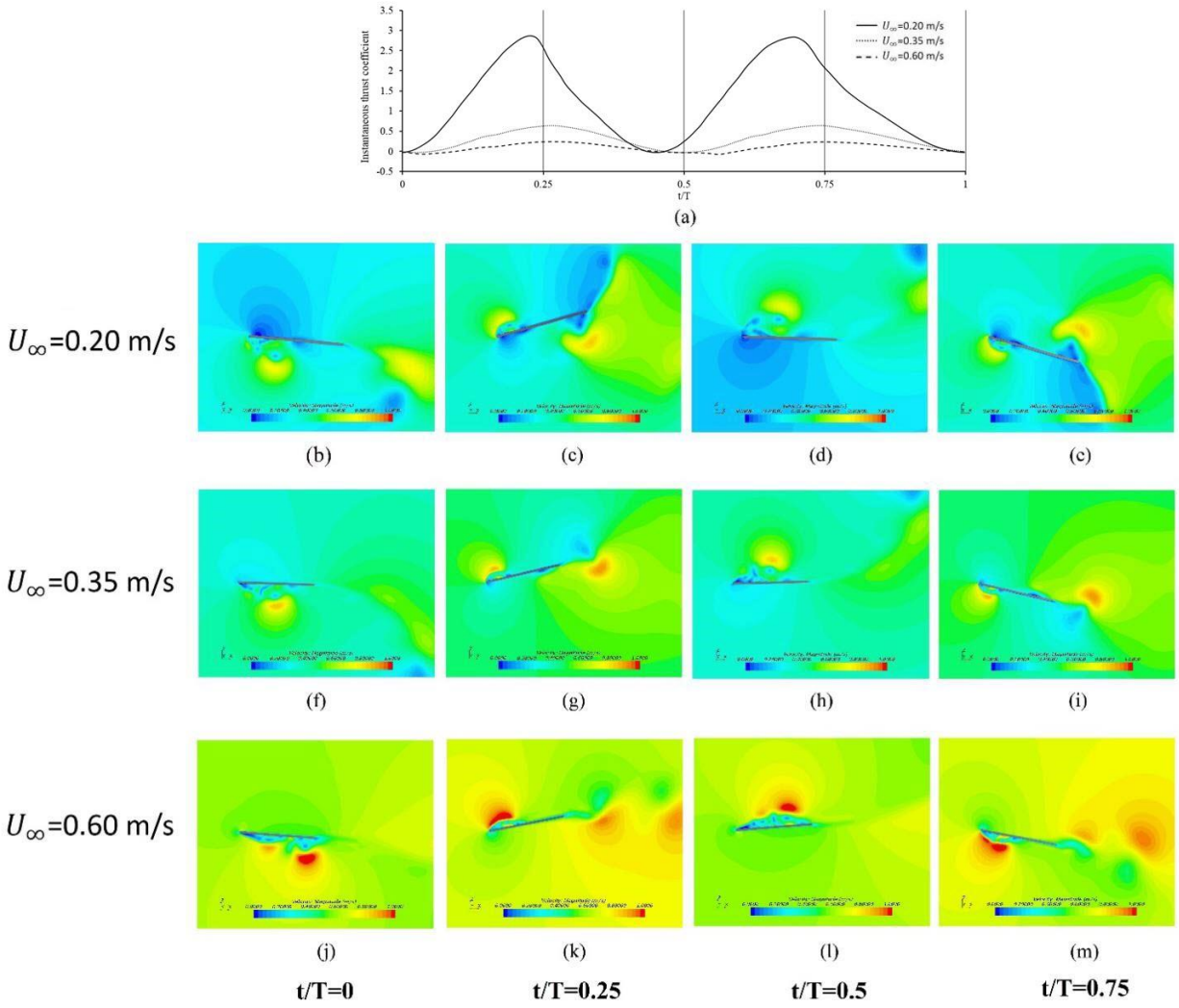

Fig.9. Evolution of instantaneous thrust coefficient and velocity contour of 2D single hydrofoil with oscillation amplitude of $\mathrm{H}/2$ and pivot position $x/c = 0$ when 2D single hydrofoil has the best propulsion performance; (a) Instantaneous thrust coefficient, the vertical solid line represent the moment of velocity contour; each row depicts various lateral velocities, for example, $(\mathrm{b})\sim(\mathrm{e})$ U_∞=0.2 m/s; each column has the same moment, for example, (b),(f),(j) t/T=0.25

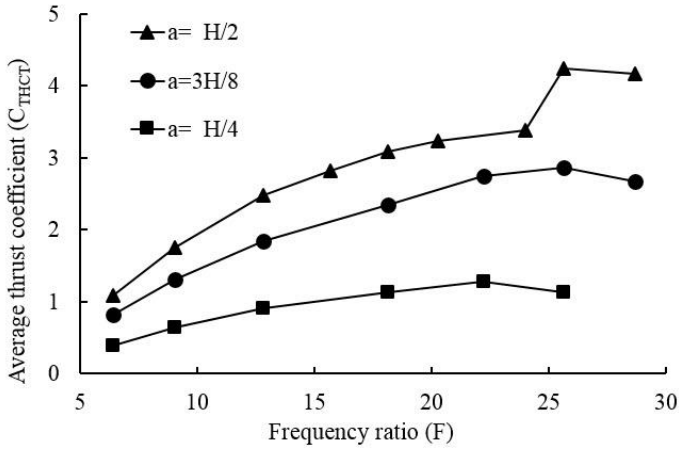

Fig.10. The average thrust coefficient of 2D tandem hydrofoils configuration under lateral velocity of 0.2 m/s and different oscillation amplitudes

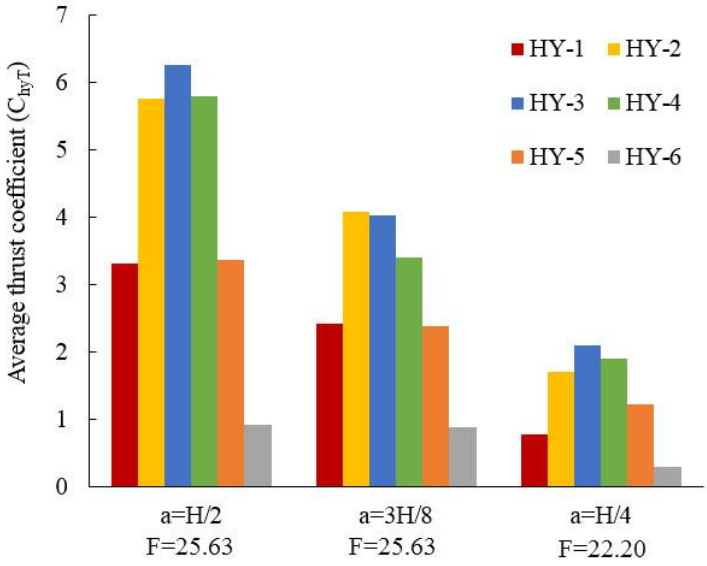

Fig.11. The average thrust coefficient of each hydrofoil under lateral velocity of 0.2 m/s and different oscillation amplitudes

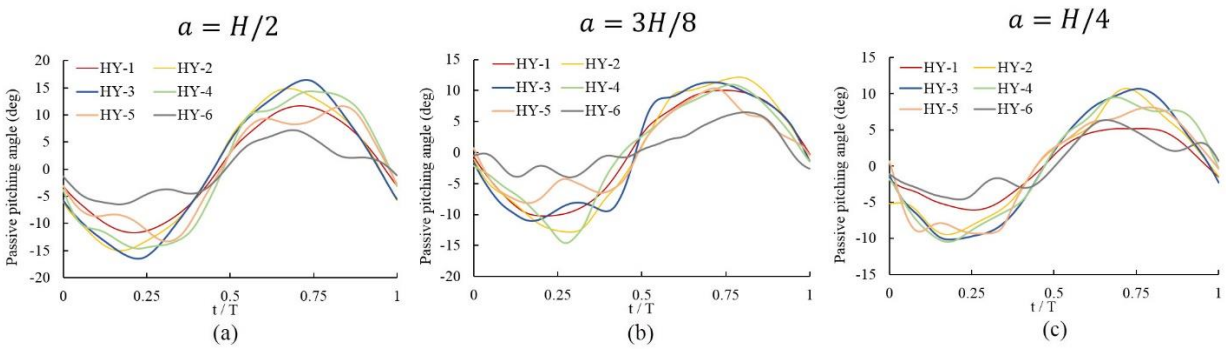

Fig.12. Variation of instantaneous passive pitching angle of 2D THC with different oscillation amplitudes when 2D tandem hydrofoils have the best propulsion performance;(a) $a = H/2$, (b) $a = 3H/8$, (c) $a = H/4$.

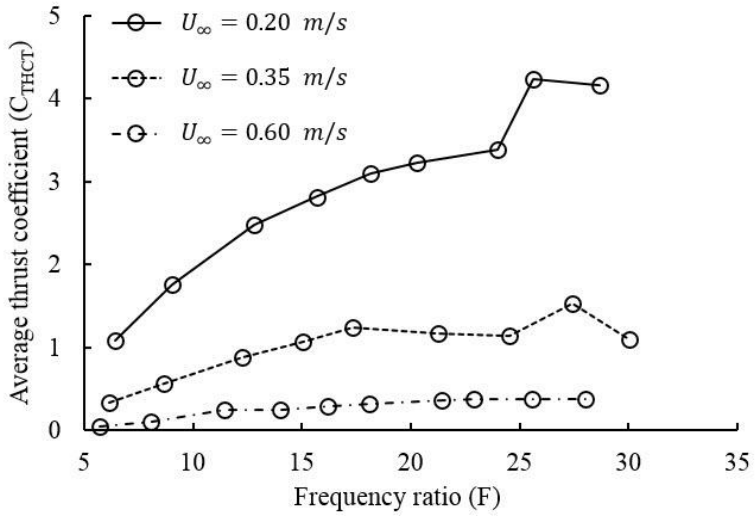

Fig.13. The average thrust coefficient of 2D tandem hydrofoils configuration under oscillation amplitudes of H/2 and different lateral velocities

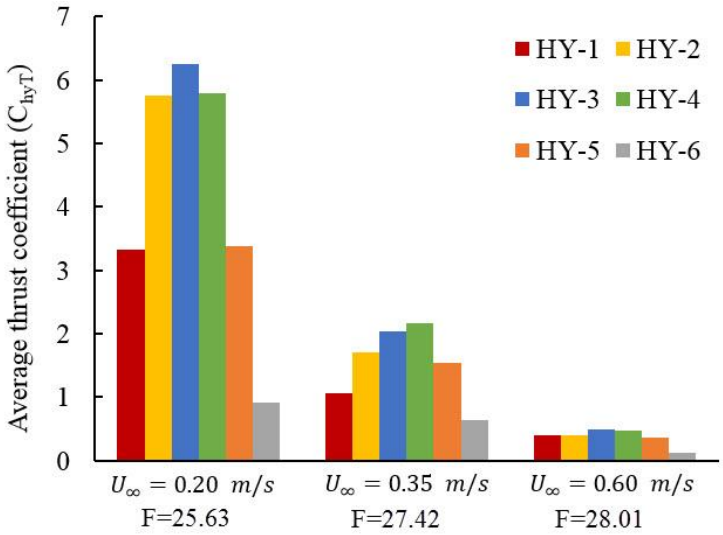

Fig.14. The average thrust coefficient of 2D tandem hydrofoils configuration under oscillation amplitudes of H/2 and different lateral velocities

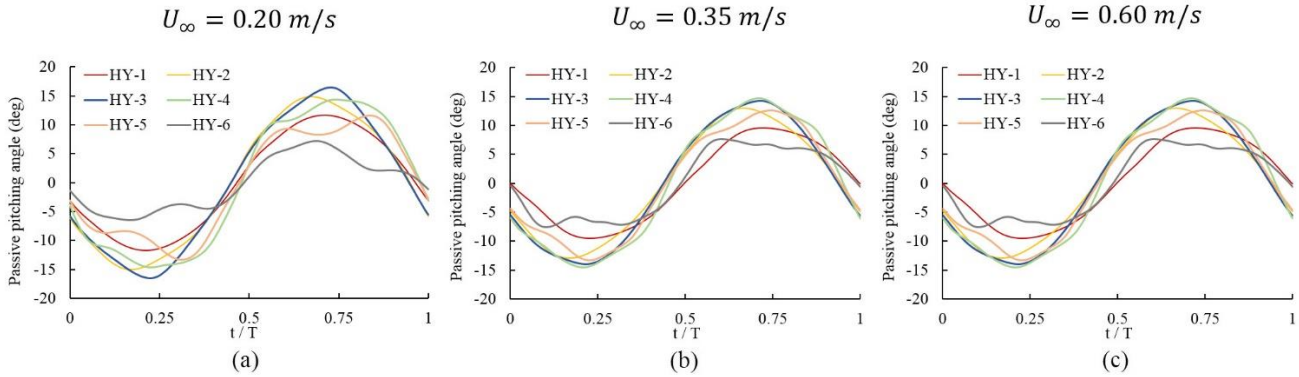

Fig.15. Variation of instantaneous passive pitching angle of 2D THC with different oscillation amplitudes when 2D tandem hydrofoils have the best propulsion performance; (a) $U_\infty = 0.20\ m/s$, (b) $U_\infty = 0.35\ m/s$, (c) $U_\infty = 0.60\ m/s$.

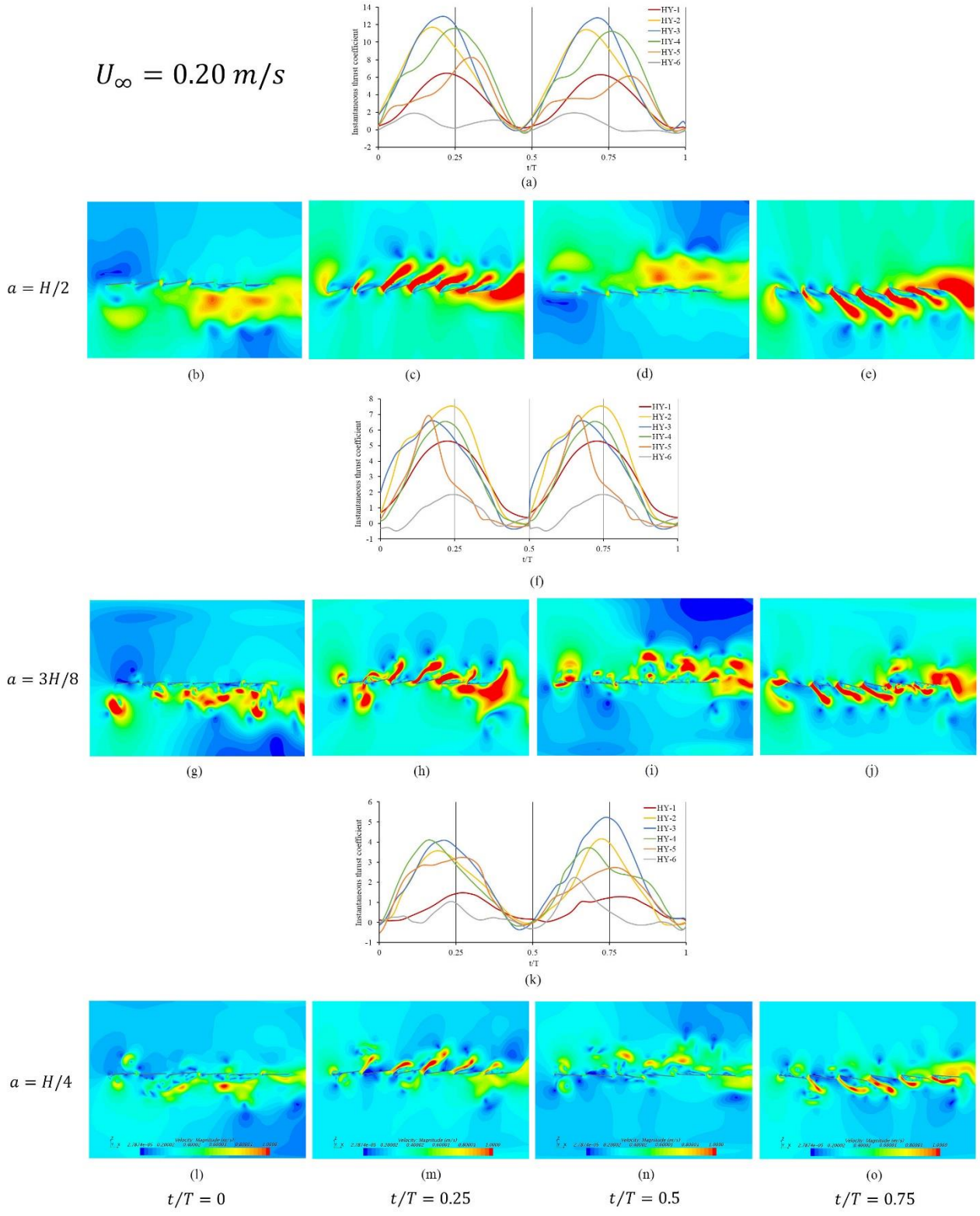

Fig.16. Evolution of instantaneous thrust coefficient and velocity contour of 2D tandem hydrofoils with different oscillation amplitudes at the lateral velocity of 0.2 m/s when 2D tandem hydrofoils have the best propulsion performance ; (a) Instantaneous thrust coefficient of six tandem hydrofoils with oscillation

amplitude of $H/2$, (f) Instantaneous thrust coefficient of six tandem hydrofoils with oscillation amplitude of $3H/8$, (g) Instantaneous thrust coefficient of six tandem hydrofoils with oscillation amplitude of $H/4$, the vertical solid line represent the moment of velocity contour; each column has the same moment, for example, (b),(g),(l) t/T=0

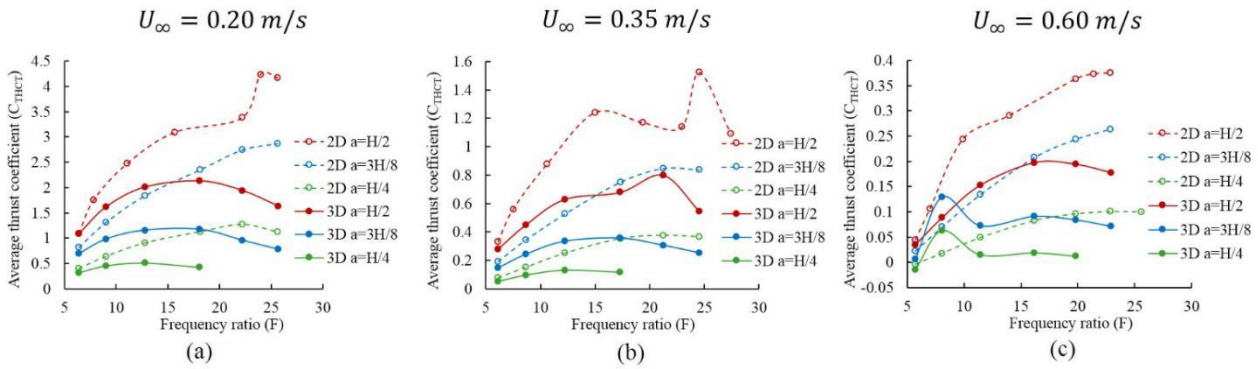

Fig.17. The average thrust coefficient of 2D and 3D six tandem hydrofoils with different oscillation amplitudes; (a) U_∞=0.2 m/s (b) U_∞=0.35 m/s (c) U_∞=0.6 m/s.

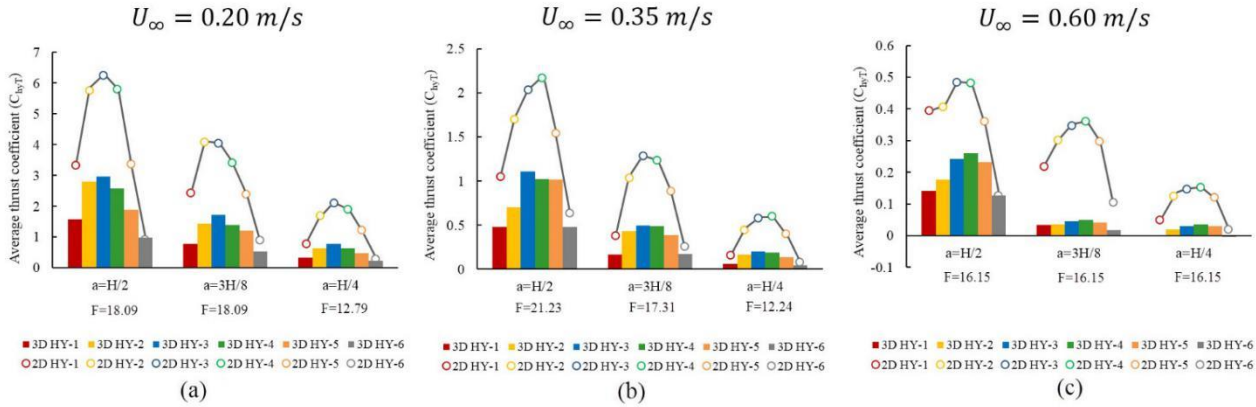

Fig.18. The average thrust coefficient of each hydrofoil in the maximum average thrust coefficient of 2D and 3D six tandem hydrofoils with oscillation amplitude of $H/2$, $3H/8$ and $H/4$; (a) U_∞=0.2 m/s (b) U_∞=0.35 m/s (c) U_∞=0.6 m/s

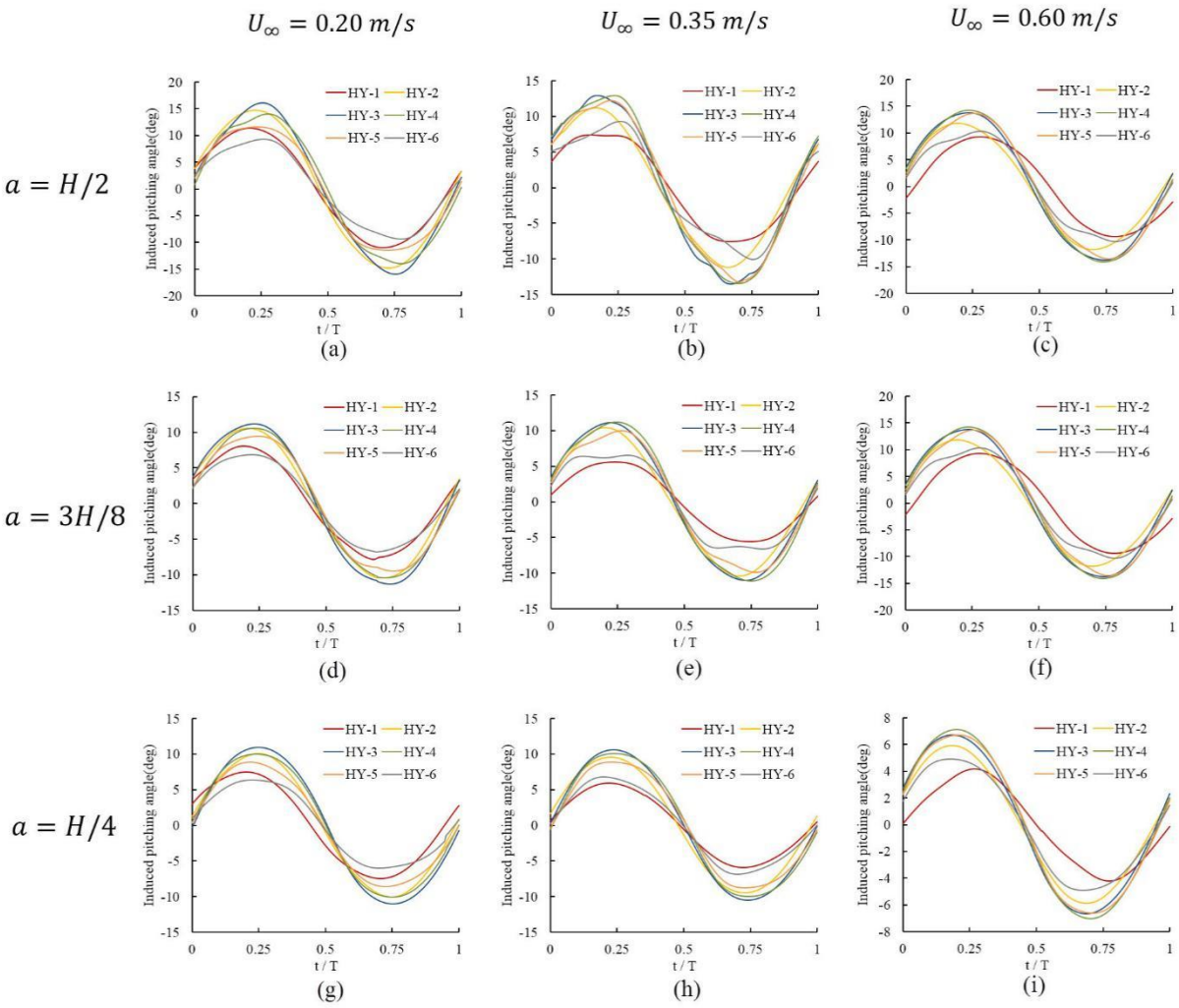

Fig.19. Variation of induced instantaneous pitching angle of 3D six tandem hydrofoils with different oscillation amplitudes when 3D six tandem hydrofoils have the best propulsion performance; the same column has the same velocity and the same row has the same oscillation amplitude;(a)~(c) $a = H/2$, (d)~(f) $a = 3H/8$, (g)~(i) $a = H/4$.

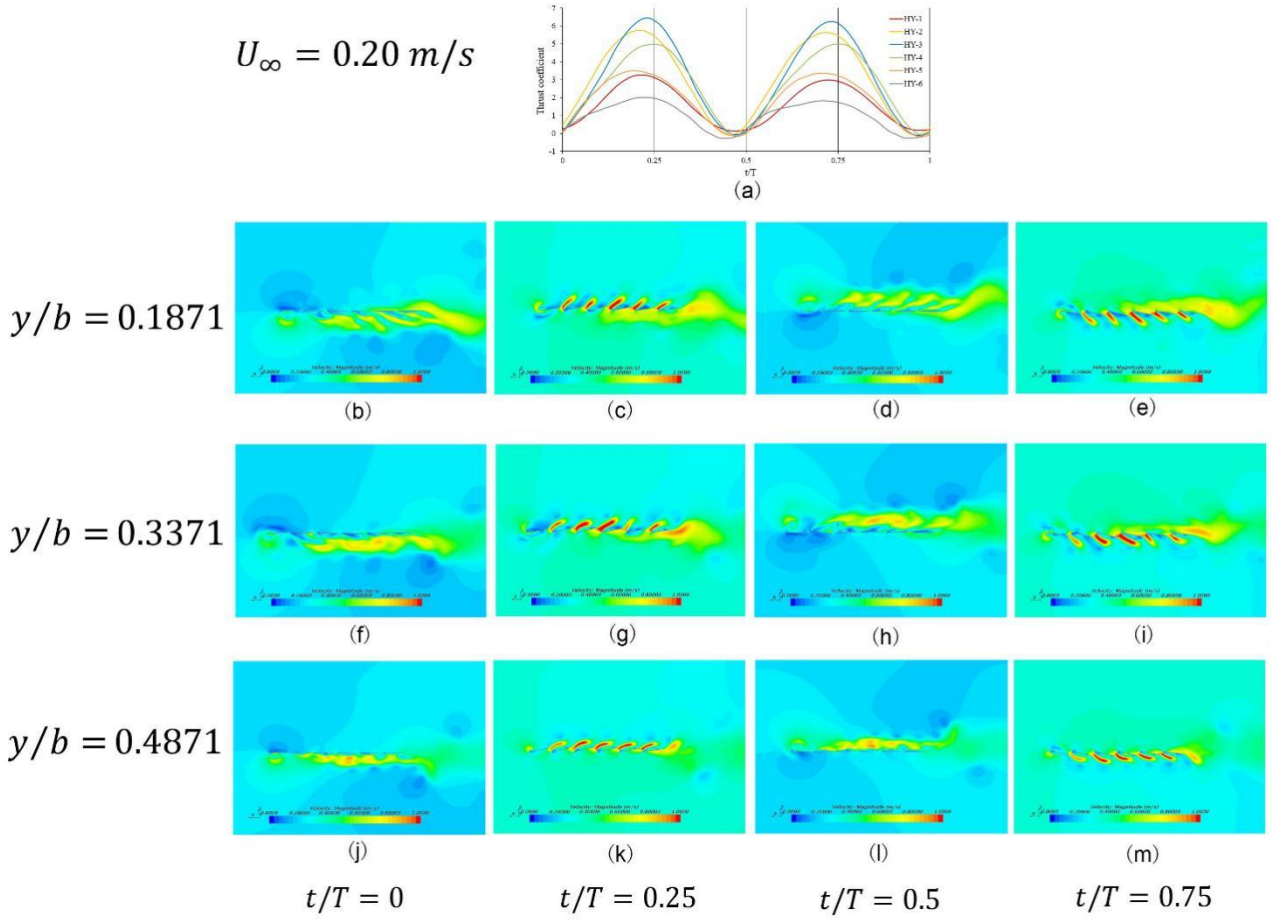

Fig.20. Evolution of instantaneous thrust coefficient and velocity contour of 3D six tandem hydrofoils with oscillation amplitude of $H/2$ at the lateral velocity of $0.20\ m/s$ when 3D six tandem hydrofoils have the best propulsion performance; (a) Instantaneous thrust coefficient of 3D six tandem hydrofoils; the vertical solid line represent the moment of velocity contour; each column has the same moment, for example, (b),(f),(j) $t/T = 0$; each row represents the same cross section of 3D tandem hydrofoils.

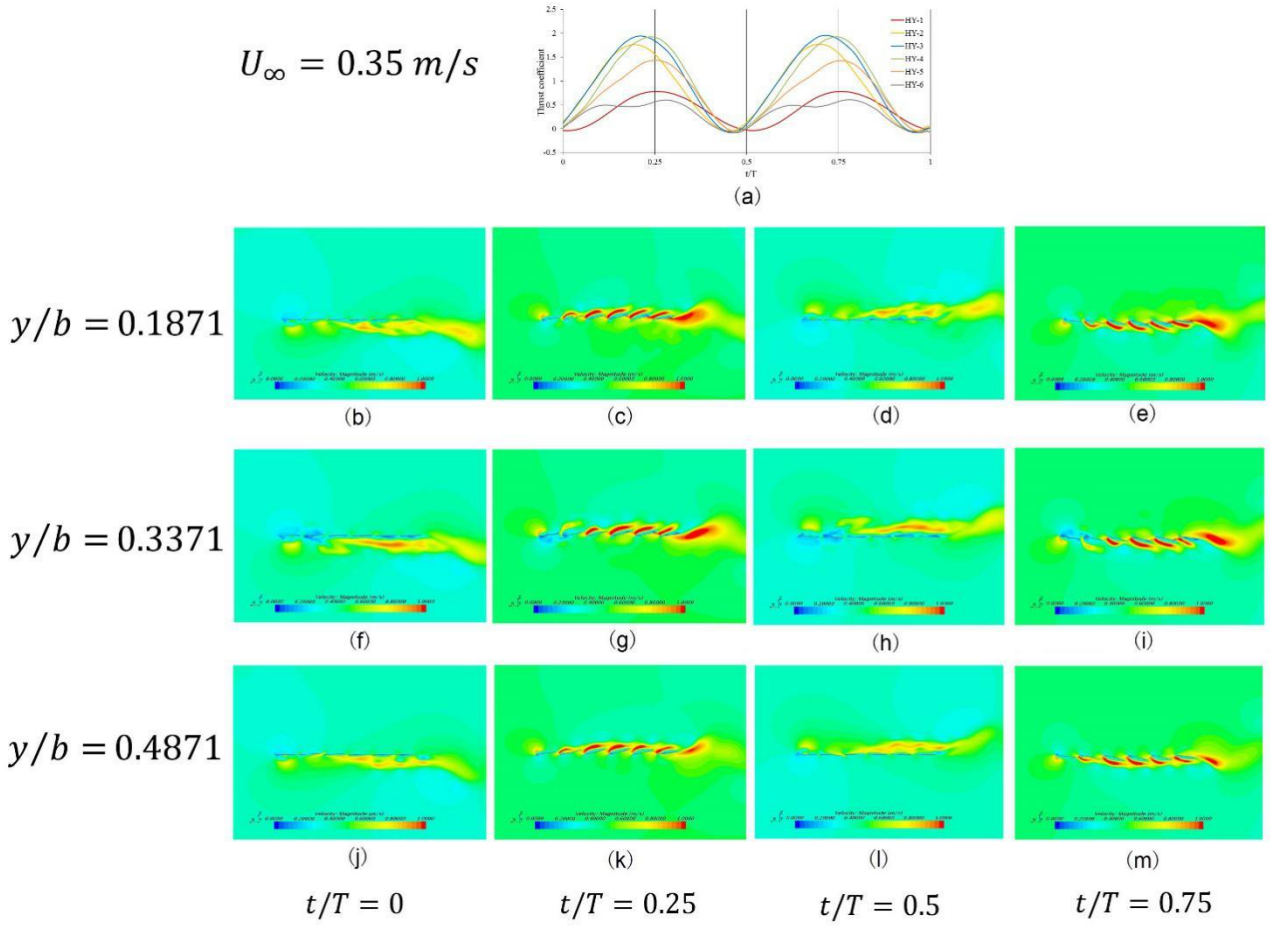

Fig.21. Evolution of instantaneous thrust coefficient and velocity contour of 3D six tandem hydrofoils with oscillation amplitude of $H/2$ at the lateral velocity of $0.35\ m/s$ when 3D six tandem hydrofoils have the best propulsion performance. (The legend is same as in Fig.20)

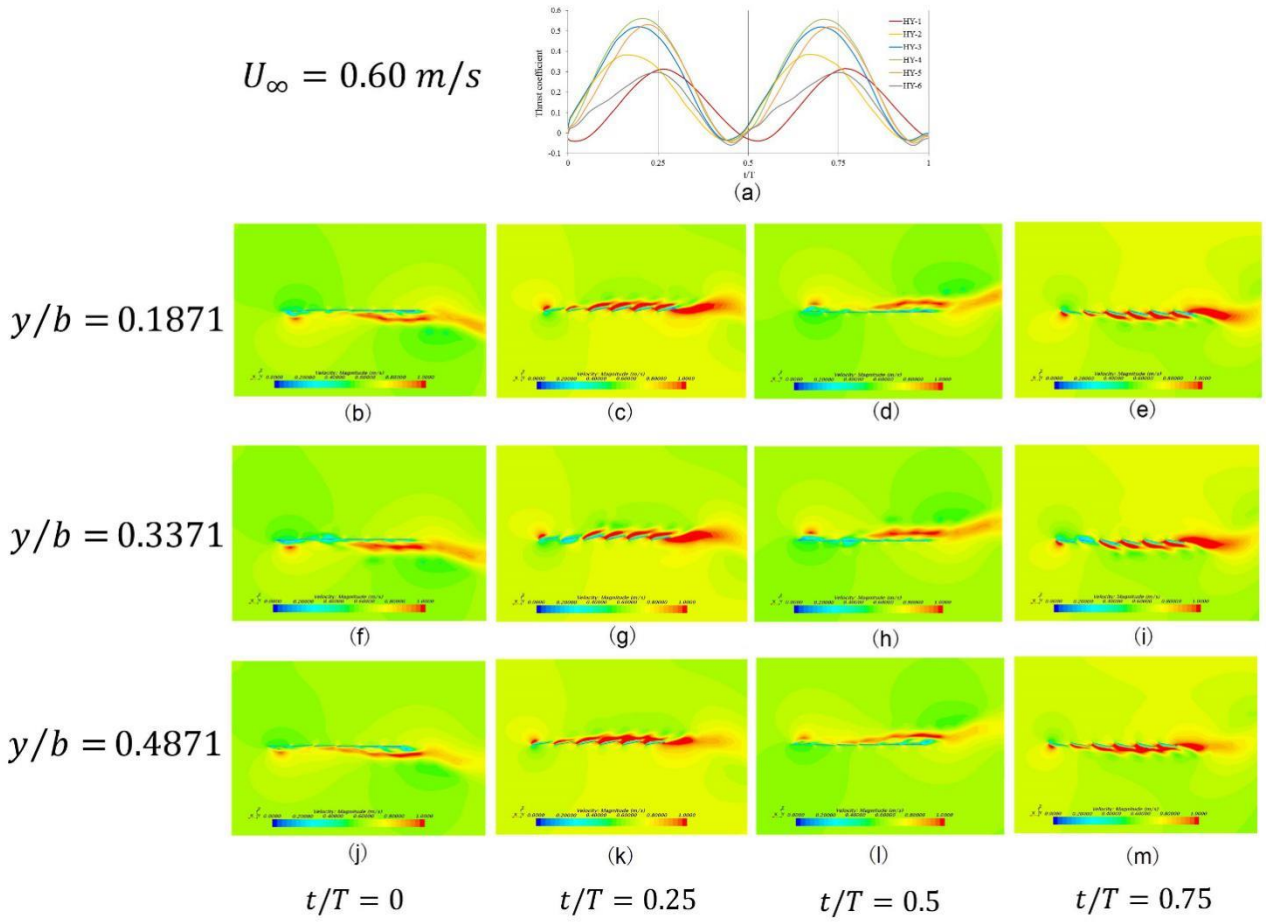

Fig.22. Evolution of instantaneous thrust coefficient and velocity contour of 3D six tandem hydrofoils with oscillation amplitude of $H/2$ at the lateral velocity of $0.60\ m/s$ when 3D six tandem hydrofoils have the best propulsion performance. (The legend is same as in Fig.20)

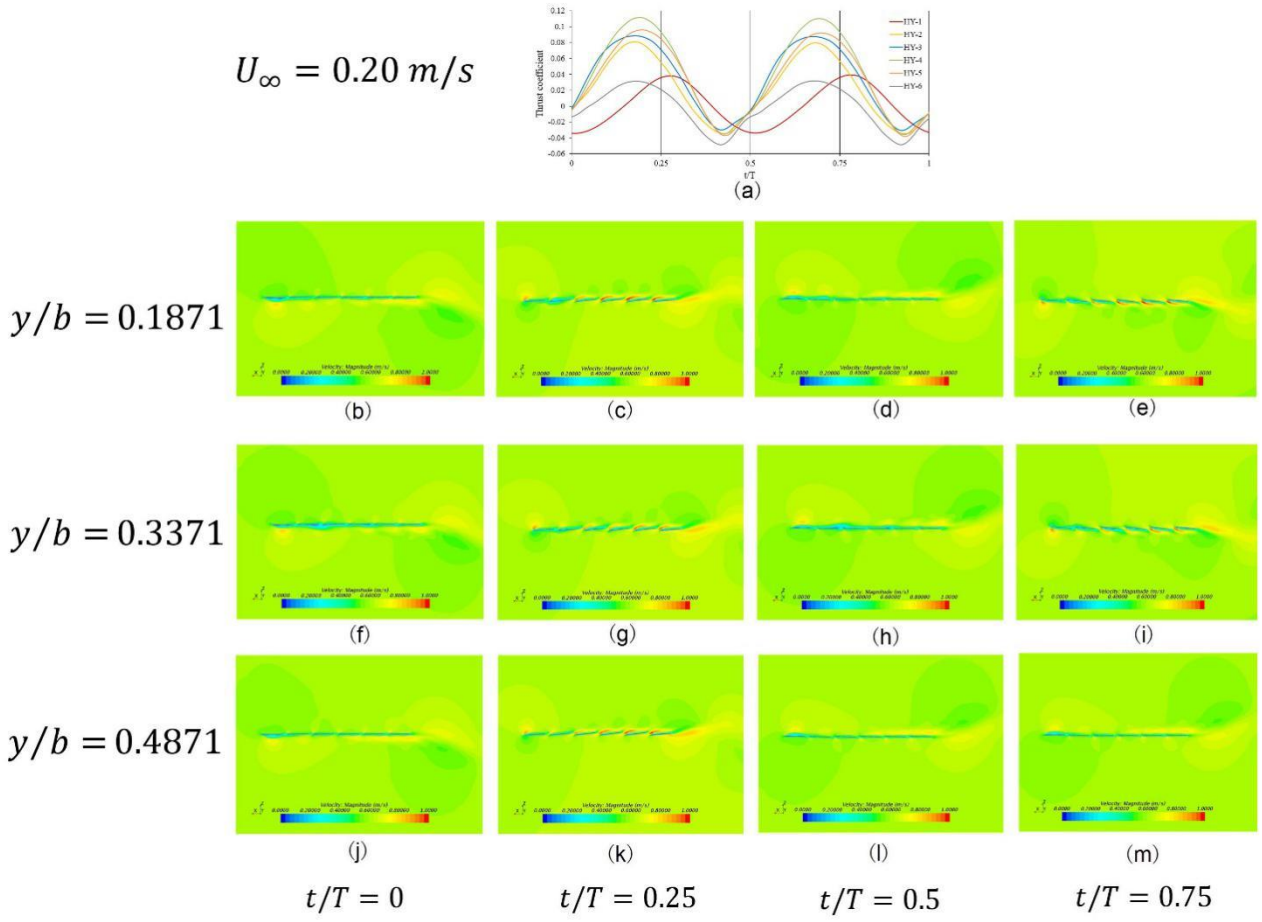

Fig.23. Evolution of instantaneous thrust coefficient and velocity contour of 3D six tandem hydrofoils with oscillation amplitude of $H/4$ at the lateral velocity of $0.20\ m/s$ when 3D six tandem hydrofoils have the best propulsion performance. (The legend is same as in Fig.20)

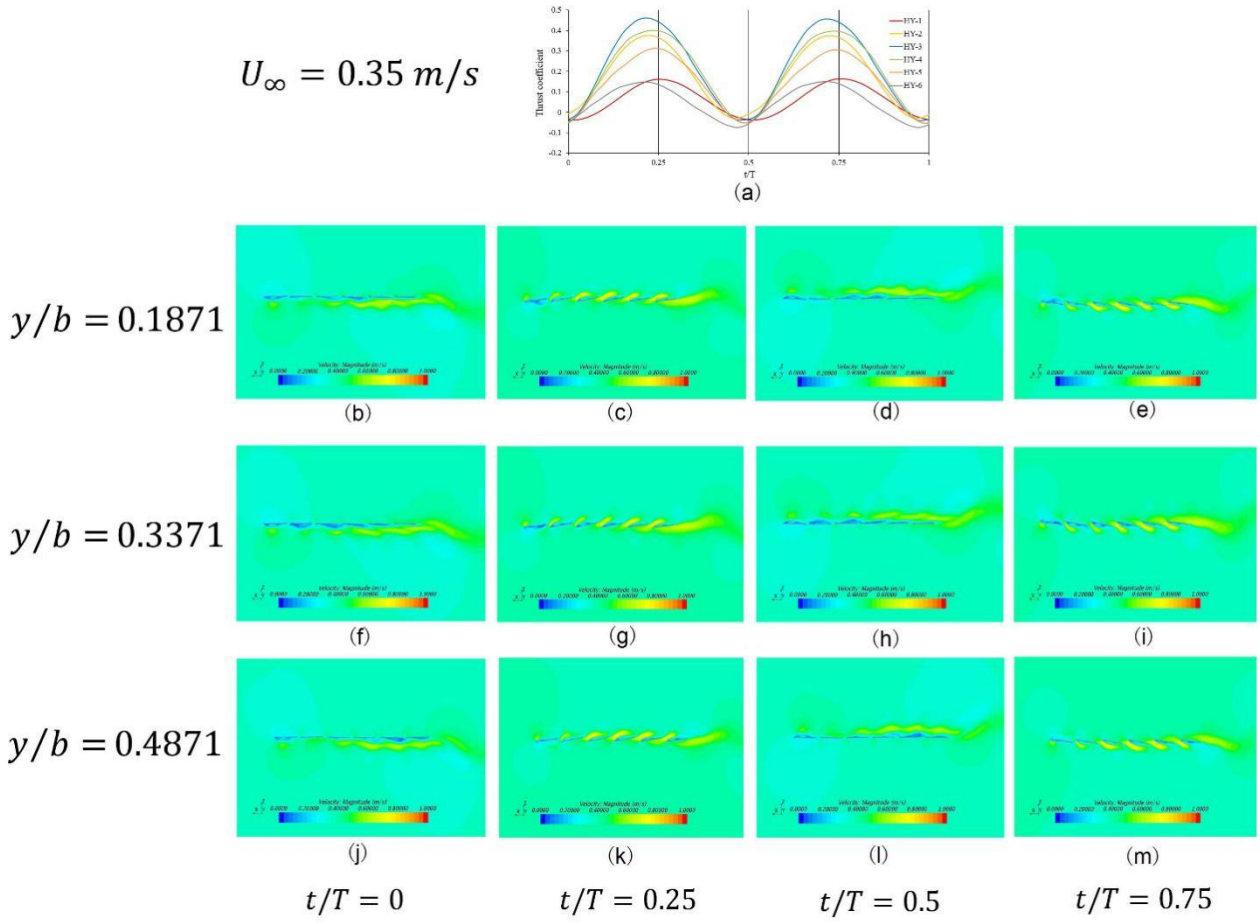

Fig.24. Evolution of instantaneous thrust coefficient and velocity contour of 3D six tandem hydrofoils with oscillation amplitude of $H/4$ at the lateral velocity of $0.35\ m/s$ when 3D six tandem hydrofoils have the best propulsion performance. (The legend is same as in Fig.20)

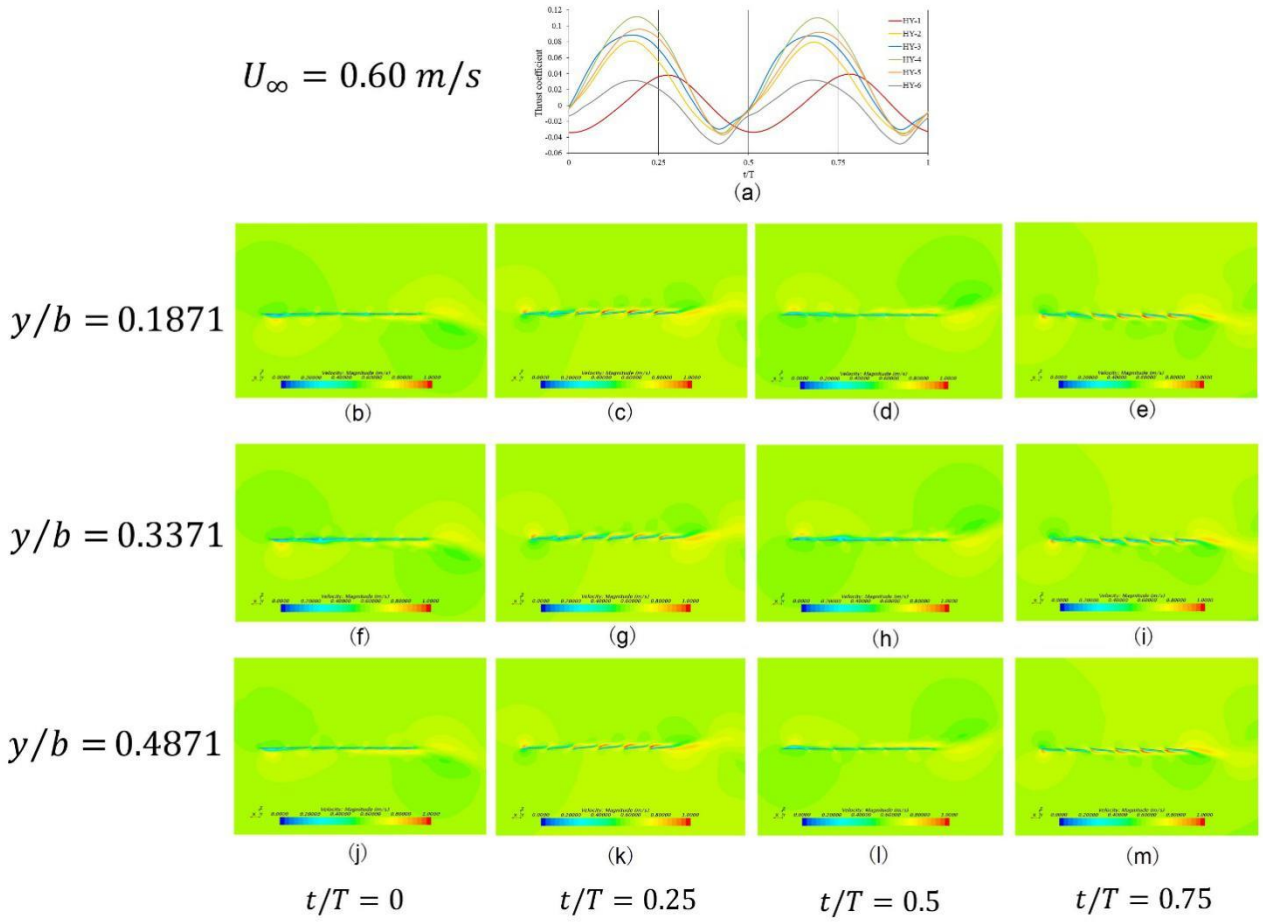

Fig.25. Evolution of instantaneous thrust coefficient and velocity contour of 3D six tandem hydrofoils with oscillation amplitude of $H/4$ at the lateral velocity of $0.60\ m/s$ when 3D six tandem hydrofoils have the best propulsion performance. (The legend is same as in Fig.20)

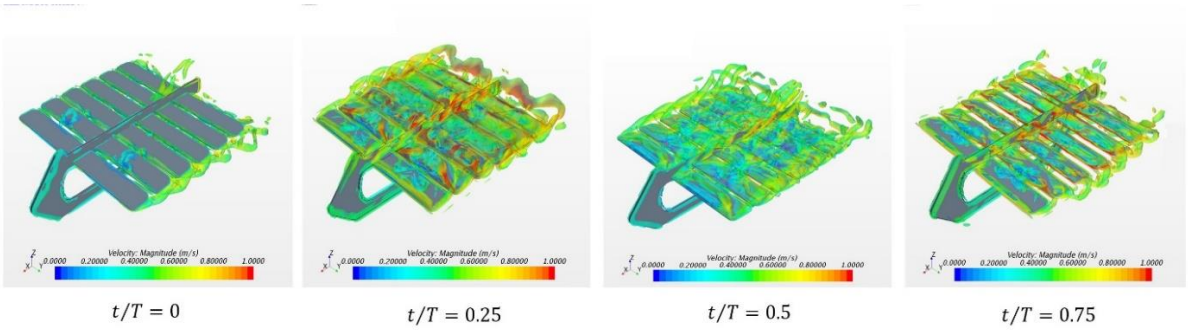

Fig.26. Evolution of instantaneous velocity contour of 3D six tandem hydrofoils with oscillation amplitude of $H/2$ at the lateral velocity of $0.35\ m/s$ when 3D six tandem hydrofoils have the best propulsion performance.

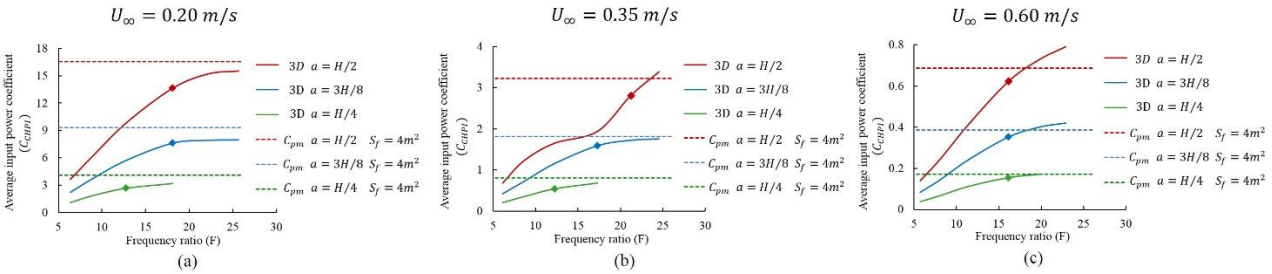

Fig.27. The average input power coefficient of 3D six tandem hydrofoils with different oscillation amplitudes; (a) U_∞=0.2 m/s (b) U_∞=0.35 m/s (c) U_∞=0.6 m/s; the frequency ratio of the diamond mark on the solid curve is equal to the frequency ratio at which the 3D six tandem hydrofoils achieves the best propulsion performance under different oscillation amplitudes.

Table 1. Characteristics of the single and tandem hydrofoils in 2D and 3D

Mesh	Cells	Vertices
Single hydrofoil (1-HC) 2D	2.37×10^5	3.08×10^5
Six tandem hydrofoils configuration (6-THC) 2D	6.22×10^5	7.45×10^5
Six tandem hydrofoils configuration (6-THC) 3D	3.93×10^6	4.28×10^6

Table 2. The maximum average thrust coefficient of 2D tandem hydrofoils under lateral velocity of 0.2 m/s and different oscillation amplitudes

	$a = H/2$	$a = 3H/8$	$a = H/4$
Frequency ratio (F)	25.63	25.63	22.20
Average thrust coefficient (C_{THCT})	4.2371	2.8707	1.277

Table 3. The maximum average thrust coefficient of 2D tandem hydrofoils under oscillation amplitude of H/2 and different lateral velocities

	$U_\infty = 0.20m/s$	$U_\infty = 0.35m/s$	$U_\infty = 0.60m/s$
Frequency ratio (F)	25.63	27.42	28.01
Average thrust coefficient (C_{THCT})	4.2371	1.5226	0.3759